# Equitable Power Grid Restoration Considering Decision Maker's Risk Tolerance

Behnam Sabzi[a], Gino J. Lim[a,*], Jian Shi[b], Saeedeh Abbasi[c]

[a] *Department of Industrial and System Engineering, University of Houston, Houston, 77204, Texas, United States*
[b] *Department of Engineering Technology and Department of Electrical and Computer Engineering, University of Houston, Houston, 77204, Texas, United States*
[c] *Optilogic, Inc., United States*

**Abstract**

This paper addresses the issue of power system restoration under uncertainty arising from climate hazards such as hurricanes, floods, and tornadoes. We propose a worst-case robust optimization model based on a graph partitioning problem to facilitate the decision-making process involved in power system restoration. In addition to the common objectives of load shedding cost and restoration time, the equity concept is integrated into the optimization model. The degree of conservativeness is incorporated to provide decision-makers with the flexibility to customize the restoration plan according to the planner's risk tolerance (i.e., risk-averse or risk-prone) regarding the unknown status of transmission lines. The model is structured as a bi-level multi-objective mixed-integer programming problem that can be solved through an iterative process. The proposed approach is tested and analyzed using three IEEE case studies of 14, 39, and 118-bus test systems. The results show that the proposed equity-aware model outperforms performance benchmark models based on a variety of performance metrics, such as average load shedding amount and average load shedding percentage.

*Keywords:*
Power System Restoration, Energy Equity, Robust Optimization, Risk Tolerance, Multi-objective optimization problem

*Corresponding Author
*Email addresses:* bsabzi@uh.edu (Behnam Sabzi), ginolim@uh.edu (Gino J. Lim ), jshi14@uh.edu (Jian Shi), saideh.abbasi@gmail.com (Saeedeh Abbasi)

**Nomenclature**

**Indices**

| | |
|---|---|
| $b$ | Index for buses, $b = 1, \ldots, NB$. $b'$ is an alias to $b$ |
| $d$ | Index for demand loads, $d = 1, \ldots, ND$ |
| $g$ | Index for black start generators, $g = 1, \ldots, NBS$ |
| $l$ | Index for transmission lines, $l = 1, \ldots, NL$ |
| $m$ | Index for sections, $m = 1, \ldots, NM$ |
| $t$ | Index for time, $t = 1, \ldots, NT$ |

**Parameters**

| | |
|---|---|
| $\omega$ | Restoration time cost rate vector |
| $\mathbf{D}$ | Real power demand vector |
| $\mathbf{KD}$ | Bus-demand incident matrix |
| $\mathbf{KG}$ | Bus-unit incident matrix |
| $\mathbf{KL}$ | Bus-line incident matrix |
| $a_{bb'}$ | Connection state between bus $b$ and $b'$ |
| $B$ | A set of buses on a network, $b \in B$, $NB = \lvert B \rvert$ |
| $c$ | Marginal cost of generators |
| $P_g^{G,min}/P_g^{G,max}$ | Minimum and maximum generating capacity of generation unit $g$ |
| $P_l^{L,max}$ | Power line capacity of line $l$ |
| $T$ | Total restoration time matrix |
| $VOLL$ | Value of loss of load |
| $x_l$ | Reactance of line $l$ |

**Variables**

| | |
|---|---|
| $\phi_t \in \mathbb{Z}$ | Auxiliary current time equal to $t$ at time $t$ |

| | |
|---|---|
| $\theta_{bt} \in \mathbb{R}$ | Phase angle of bus $b$ at time $t$ |
| $LS \in \mathbb{R}$ | Load shedding vector per demand (hourly) |
| $n_m \in \mathbb{Z}$ | The number of buses in section $m$ |
| $P_{gt}^G \in \mathbb{R}$ | Generated power of unit g at time $t$ |
| $P_{lt}^L \in \mathbb{R}$ | Power flow on line $l$ at time $t$ |
| $s_{bm} \in 0, 1$ | State of bus $b$ at section $m$ |
| $T_d^{load} \in \mathbb{Z}$ | Load pick up time of demand $d$ |
| $y_{bb'} \in 0, 1$ | Tie-line state between bus $b$ and $b'$ |
| $LS' \in \mathbb{R}$ | Load shedding vector per section (hourly) |

## 1. Introduction

Environmental hazards, including hurricanes, floods, and tornadoes, pose an increasing threat to the reliable operation of the power grid, exacerbated by climate change [1, 2]. Additionally, aging power grid infrastructure further heightens vulnerability to adverse weather conditions [3]. In the United States alone, severe weather events caused 891 power outages between 2014 and 2018, with the major winter storm in February 2021 leading to a prolonged outage affecting over four million customers in Texas [4]. On average, electricity customers in the U.S. experience approximately 250 minutes of power loss annually, with 138 minutes attributed to major weather events such as snowstorms, hurricanes, floods, and heatwaves [4]. These outages impose significant reliability challenges and financial burdens on communities, specially those ones not have sufficient resource to cope with such disasters. The inflation-adjusted cost of weather-related power outages in the U.S. is estimated at $27 billion annually [5].

Beyond economic and operational consequences, power restoration raises critical equity concerns. Equity refers to the fair distribution of benefits and burdens across communities, ensuring that populations with limited resource are not disproportionately affected. Energy justice extends this principle by advocating for universal access to affordable, reliable, and sustainable energy services. Equity-aware power restoration is essential to mitigating the disproportionate impacts of extreme weather events and fostering a more just energy system [6].

Statistics have shown that compared with other communities, communities with limited access to resources and infrastructures bear a disproportionate burden of the severe impacts of extreme weather events. These communities often lack influence in the decision-making process related to their energy services, resulting in unfavorable restoration processes that leave them in the dark for days, or even weeks. Equity-related concerns have long been neglected in the context of power restoration [7, 8, 9, 10]. Common objectives found in the literature include load shedding cost ([11, 12, 13, 14, 15]), restoration time ([11, 12, 13, 16]), power generation cost [12], system energizing capability ([17, 14, 15]), and load curtailment [17]. However, to achieve an equitable energy future, energy justice principles such as fairness and social equity must be integrated into energy systems. Addressing these principles in the power restoration process is crucial to ensuring that all communities are prioritized and treated equitably during and after extreme weather events.

Following a complete or partial failure, power systems must be restored to normal operation as quickly as possible. Power restoration can be done sequentially or in parallel. The sequential restoration process typically follows a sequence of steps, which can be time-consuming. In comparison, a parallel power system restoration strategy can be more advantageous, especially for widespread blackouts [12, 18, 19, 20]. During parallel restoration, the affected area is sectionalized into smaller subsystems at the early stages of restoration. These separate sectionalized subsystems will then be restored through careful coordination, based on their generator ramping capabilities, penetration levels of renewable energy sources (RES), and load recovery requirements [21, 17]. All the subsystems will be reconnected in the last stage to rebuild the entire system by re-energizing transmission lines and substations [18, 20].

However, designing an effective and prompt restoration strategy is not straightforward. One such major challenge is associated with uncertainties, especially with an ever-increasing penetration of renewable energy sources that can be highly stochastic and volatile. By employing data-driven, quantitative metrics, recent studies have captured the uncertainty inherent in network disruptions and recovery processes [22]. Although appropriate preparation and prior planning can help enhance and accelerate the power restoration process, various sources of uncertainties must be carefully considered during the restoration process [23, 24], which include load forecast [25, 26, 27], renewable energy resources [28], infrastructure damage [29], and line availability [13]. Among various uncertainties in power systems, transmission line outages are particularly concerning due to their high vulnerability

to natural disasters. This is because transmission lines are typically exposed in wide-open areas, making them more susceptible to damage. When a hurricane strikes a power network, the availability of power transmission lines varies widely depending on the intensity of the hurricane and the resilience of the impacted facilities [30]. Therefore, the condition of those damaged lines needs to be incorporated from the beginning of the power restoration process to ensure a speedy recovery.

So far, most studies in the literature have focused on simulating the failure of the transmission lines and its impact after a disruption [31, 32]. To this issue, probabilistic studies have been conducted to predict the occurrence of a disruptive event leading to transmission line failure [31, 32]. An unsupervised deep learning framework was proposed in [33] to detect power transmission line faults, while considering uncertain parameters. Furthermore, uncertainty associated with transmission line outages has also been studied in transmission expansion problems. For instance, [34] presents a stochastic model that coordinates the planning of generation and transmission expansion, while taking into account random outages of transmission lines. Additionally, [35] incorporates random uncertainties in transmission lines when addressing the problem of generation and transmission line expansion planning. However, the uncertain nature of line failures, following a disruption event, has been largely left unaddressed in the power restoration literature.

While robust optimization (RO) approaches have recently been proposed to account for uncertainties in transmission line availability, these models often adopt a worst-case perspective that treats all uncertain outcomes with equal weight [36, 37, 38]. This can lead to overly conservative solutions that may unnecessarily limit operational flexibility or overcommit restoration resources. Existing models typically lack a mechanism to calibrate the level of conservatism based on the likelihood of line availability or the decision-maker's tolerance for risk. This gap highlights the need for a more flexible framework that allows planners to tailor restoration strategies to different risk profiles. Introducing a tunable parameter to represent the degree of conservativeness provides a practical way to bridge this gap, enabling a smoother trade-off between robustness and efficiency under uncertainty.

To bridge these two important research gaps identified above, in this paper, we develop a novel approach to facilitate the cost-effective, equitable, and prompt parallel restoration of a power grid. While uncertainties can be modeled by stochastic programming (SP) [39], [40, 41], robust optimization [14, 42, 43], and risk-constrained methods [44], as the probability distribution of the line damage is often unknown/hard to forecast, we consider an

RO approach that constructs a solution that is feasible for any possible realizations of the parameter within an assumed uncertainty set to cover a variety of failure scenarios based on a limited amount of data [45, 46, 47]. First, we formulate a bi-level graph partitioning problem (GPP) as the base model, with equity taken into account. Then, we develop a worst-case robust optimization (RO) model to take into account the uncertainty of transmission line status following a natural disaster, where the fragility curve is used to estimate transmission line failure at a given wind speed [48]. Lastly, we elaborate on the degree of conservativeness concept, which provides decision-makers with the flexibility of adjusting the restoration plan according to the operator's risk tolerance.

The contributions of this work are three-fold:

- *Equity-aware problem formulation*: A novel equity-aware bi-level formulation is proposed in this paper to restore power considering economic and social disparities among various communities. The model introduces network flow constraints to address the infeasibility issue found in [13].
- *Worst-case robust optimization model*: A worst-case RO model is proposed to develop a reliable power system restoration plan under the uncertainty of transmission line availability.
- *Adjustable degree of conservativeness for flexibility in planning*: A concept of degree of conservativeness is introduced to help decision-makers develop a post-hurricane restoration plan according to their risk-taking preferences on the parameter uncertainty.

The rest of the paper is organized as follows. Section 2 describes the problem and the optimization model formulations in four steps: the equity indexes (2.1), the equity aware deterministic model (2.2), the robust counterpart model (2.3), and the degree of conservativeness on the line failure (2.4). Section 3 discusses numerical experiments, and conclude the paper in Section 4.

## 2. Problem Description

This work builds upon the graph partitioning problem (GPP) model introduced in [13], which serves as our benchmark. One critical limitation of the existing GPP model is its inability to guarantee feasible power flow throughout the network. Specifically, due to the formulation's lack of explicit

constraints ensuring connectivity between nodes and at least one generator, the model may lead to infeasible solutions, as illustrated in Figure 1(b). To overcome this issue, we introduce additional network flow constraints to the GPP formulation, ensuring that all partitioned regions maintain a viable power connection.

This study assumes that power restoration follows a build-up restoration approach, as described in [49]. In this approach, the grid is decomposed into smaller sub-networks, and restoration is conducted within each partition before potential reconnection. It is important to note that the reconfiguration process necessary to merge these restored regions is beyond the scope of this work.

To model the problem effectively, we formulate the GPP as a bi-level optimization problem. The upper-level model (see constraints (11)-(23)) is responsible for partitioning the power network into multiple regions, each containing exactly one black-start (BS) generator—an emergency power source capable of operating independently of the main grid [50]. Based on the partitions determined in the upper level, the lower-level model (see constraints (26)-(36)) focuses on energizing each of the resulting sub-networks while ensuring feasible power flow.

Given the complexity of the problem, multiple, and often conflicting, objectives must be considered. For instance, maximizing power supply minimizes load shedding but increases power generation costs. To handle these trade-offs, we adopt a preemptive goal programming approach [51], which enables prioritization among conflicting objectives. The upper-level model aims to minimize the number of connections between subsections (promoting a modular design), load-shedding costs, restoration time costs, and power generation costs. The lower-level model retains all upper-level objectives, except for the line connection cost, while incorporating additional line power flow constraints.

In the following sections, we focus on the integration of equity considerations into the power restoration process, presenting the mathematical formulations of the proposed models in a structured manner. We begin by discussing the equity indices employed in this work in Section 2.1: Theil's T index, utilized as an equity performance measure in the upper-level model, and the equity gap, incorporated as an additional equity measure at the lower level. Theil's T index, which captures disparities in resource allocation, involves a logarithmic function that complicates direct computation. To address this challenge, we derive a second-order Taylor's approximation, which, while not linear, simplifies the computational complexity of the problem. Similarly, the equity gap measures inequities across different communi-

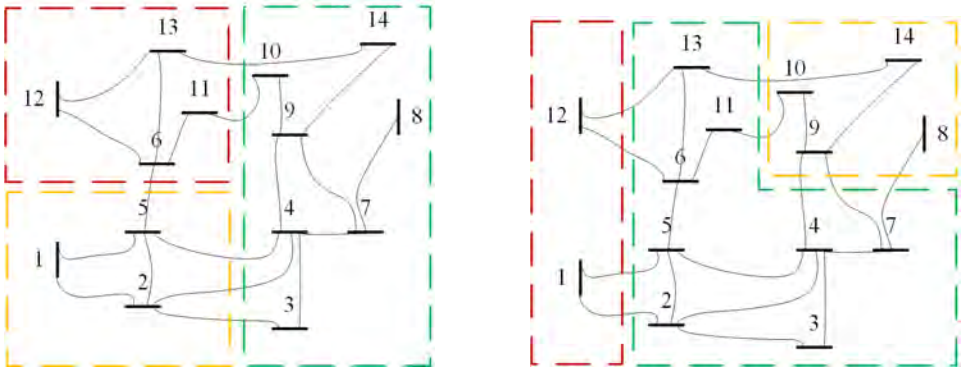


(a) An example of feasible sectionalization (b) An example of infeasible sectionalization

Figure 1: Analysis of the influence of different economic policies

ties, ensuring a holistic approach to equity in the restoration process.

Next, Section 2.2 introduces the Equity-aware GPP model, a deterministic and simpler formulation that incorporates equity measures directly into the bilevel preemptive goal programming framework. This model replaces traditional objectives such as load-shedding cost with equity-driven objectives to ensure a fair distribution of resources during the restoration process.

Following this, we extend the Equity GPP model to develop its robust counterpart, the Equity RCP model in Section 2.3, which accounts for worst-case scenarios. This model introduces a modification to the bus connection matrix $a^s_{b,b'}$ to address uncertainties associated with extreme events. The robust formulation ensures that equity considerations remain effective even under highly uncertain and adverse conditions.

Finally, we define the degree of conservativeness in Section 2.4, represented by the parameter $\delta$, as a measure of decision-makers' risk tolerance. This parameter governs the perception of failed lines caused by extreme events by incorporating wind speed scenarios into the connectivity matrix. It provides decision-makers with flexibility in adjusting the restoration plan according to their risk tolerance, enabling a trade-off between the conservativeness of the solution and the restoration objectives, and concluding the mathematical section of the paper.

### *2.1. Equity Indexes*

Various metrics have been developed to measure equity in resource distribution, each with its own advantages and limitations. In this work, we utilize Theil's T index [52] and the equity gap to assess equity in power grid

restoration. Theil's T index, specifically its between-zone index (BZI) component, is employed at the upper level to capture disparities in load shedding across different grid sections. At the lower level, we use the equity gap to ensure that deviations in load shedding within each section remain minimal, maintaining fairness among different loads in the same section.

While Theil's T index includes both BZI and within-zone index (WZI) components [52], we do not use WZI at the lower level because it introduces nonlinearity and non-convexity into the problem. In a bilevel formulation, ensuring convexity in the lower level is crucial for convergence, making the equity gap a more suitable choice for maintaining equity within sections while keeping the problem tractable.

*2.1.1. Theil's T Index*

Theil's T index is an entropy-based measure of inequality in the distribution of a scarce resource [52]. In this study, the scarce resource is load shedding, and our goal is to ensure that load shedding is distributed as equitably as possible across different sections of the power grid. Theil's T index is particularly well-suited for this application because it not only quantifies overall inequality but also allows for decomposition into between-zone inequality (BZI) and within-zone inequality. The BZI component captures how much of the total inequality is due to disparities between different sections of the grid, enabling a more granular analysis of equity [6].

Unlike threshold-based metrics, which only ensure a minimum level of service, or min-max approaches, which may be skewed by outliers, Theil's T provides a more comprehensive equity assessment. Its decomposability allows us to evaluate disparities between different sections, highlighting areas that experience disproportionately high load shedding and enabling targeted mitigation strategies. Additionally, Theil's T is transformable into relative measures, making it easier to interpret and compare across different grid conditions. By minimizing Theil's T, we aim to achieve a more equitable distribution of load shedding, ensuring that no section of the grid bears a significantly higher burden than others.

The general formula for the between-zone component is given as:

$$BZI = \sum_{k=1}^{K} y_k \ln(\frac{\bar{x}_k}{\bar{x}}) \tag{1}$$

where $K$ is the number of sections (in our case, $K = NG$, the number of black-start generator zones), $y_k$ is the ratio of the total resource allocated to zone $k$ relative to the entire system, $\bar{x}_k$ is the mean amount of resource

allocated to each node in zone, and $\bar{x}$ is the overall mean amount of resource allocated per node in the entire system. If the $BZI$ is close to zero, it indicates near-perfect equality. As $BZI$ increases towards 1, it indicates growing inequality.

In this problem, the resource under consideration is load shedding. Suppose we have three sections (e.g. 14-bus case study) and let $\bar{x_1}$, $\bar{x_2}$, and $\bar{x_3}$ represent the load shedding in each of these three sections. The total load shedding in the system is $p = \bar{x_1} + \bar{x_2} + \bar{x_3}$. The mean load shedding per section in the entire system is $\bar{x} = \frac{\bar{x_1}+\bar{x_2}+\bar{x_3}}{3} = \frac{p}{3}$. The ratio of load shedding in section $k$ to the total system load shedding is:

$$y_k = \frac{\bar{x}_k}{\bar{x_1} + \bar{x_2} + \bar{x_3}} = \frac{\bar{x}_k}{p}, k \in 1, 2, 3 \tag{2}$$

Substituting these terms into the between-zone equality formula, we have:

$$BZI = \sum_{k=1}^{3} \frac{\bar{x}_k}{p} \ln(\frac{3\bar{x}_k}{p}) \tag{3}$$

Thus, if the goal is to minimize the total inequality across all three sections, the objective function becomes as minimization of equation 3.

Optimizing such a nonlinear formulation directly can be challenging, as it involves a logarithmic term. To address this, a Taylor series expansion around a chosen point $\hat{x}$ can be applied to linearize or approximate the objective. First, we derive the Taylor's expansion for one of the sections. we define $z_1$ as Theil's T index of section 1.

$$z_1 = \frac{\bar{x}_1}{p} \ln(\frac{3\bar{x}_1}{p}) \tag{4}$$

consider the Taylor expansion around $x_1 = \hat{x}$. After performing the Taylor's expansion and collecting terms, we arrive at an approximate form for $z_1$:

$$z_1 \approx \frac{1}{2p\hat{x}}(\bar{x}_1 + \hat{x} \ln \frac{3\hat{x}}{p})^2 - \frac{\hat{x}(\ln^2 \frac{3\hat{x}}{p} + 1)}{2p} \tag{5}$$

This approximation transforms the problem into a more tractable form. Applying the same process to $z_2$ and $z_3$, the total approximate objective function becomes:

$$\begin{aligned} BZI \approx \frac{1}{2p\hat{x}} \Big[ & (\bar{x}_1 + \hat{x} \ln \frac{3\hat{x}}{p})^2 + (\bar{x}_2 + \hat{x} \ln \frac{3\hat{x}}{p})^2 + \\ & (\bar{x}_3 + \hat{x} \ln \frac{3\hat{x}}{p})^2 \Big] - \frac{3\hat{x}(\ln^2 \frac{3\hat{x}}{p} + 1)}{2p} \end{aligned} \tag{6}$$

Choosing the right expansion point $\hat{x}$ is critical for a good approximation. By taking the derivative of the approximate function with respect to $\bar{x}_1$(and similarly for other variables) and setting it to zero, we can find the stationary point. The $\frac{dBZI}{d\hat{x}}$ leads to the conclusion that $\hat{x} = \frac{\exp(-1)}{3}$.

Since the last term and $\frac{1}{2p\hat{x}}$ in equation (6) are constants, we can omit them from the objective function. We further approximate $BZI$ by replacing $\hat{x}$ with $\frac{\exp(-1)}{3}$ in equation (6):

$$\begin{aligned}\widehat{BZI} = \Bigg[&(\bar{x}_1 - \frac{\exp(-1)}{3})^2 + \\ &(\bar{x}_2 - \frac{\exp(-1)}{3})^2 + (\bar{x}_3 - \frac{\exp(-1)}{3})^2\Bigg] = \\ &\sum_{k=1}^{3}(x_k - \frac{\exp(-1)}{3})^2 \end{aligned} \tag{7}$$

The above formulations enable the integration of Theil's T index into a power grid restoration optimization model by approximating its nonlinear, nonconvex logarithmic terms. This facilitates its use within a bi-level goal programming framework, offering a practical approach to incorporating equity considerations into complex infrastructure decision-making.

*2.1.2. Equity Gap Index*

To address equity in the lower-level optimization problem, we use the equity gap metric. As mentioned earlier, incorporating the WZI component of Theil's T index would introduce nonlinearity and non-convexity, which pose challenges in solving a bilevel optimization problem. Instead, we adopt the equity gap approach to maintain convexity while ensuring fairness in resource allocation within each section.

The equity gap captures the disparity between the entities receiving the highest and lowest amounts of a resource. To minimize this gap, we introduce the following objective function:

$$\min f^{EA} = x_{max} - x_{min} \tag{8}$$

where $x_{max}$ represents the maximum resource allocated to any entity in the system, and $x_{min}$ represents the minimum allocation. To define these values, we introduce the following constraints:

$$x_{max} \geq x_i, \forall i \tag{9}$$

$$x_{min} \leq x_i, \forall i \tag{10}$$

Later in our mathematical formulations, we replace $x$ with $LS$, $x_{max}$ with $LS_{max}$, and $x_{min}$ with $LS_{min}$ for both the equity gap and Theil's T index formulation. This structured approach ensures equity within each section while keeping the lower-level problem tractable.

*2.2. Equity based GPP Model*

This is the first section that we are going to discuss about the basic GPP model. The GPP at the upper level aims to optimize the restoration process by minimizing (11) the amount of load shedding, (12) restoration time, (13) the cost of power generation, and (14) the objective term of the GPP. The objective term of the GPP aims to minimize the number of tie-lines between different sections of the grid to facilitate the process of grid segmentation. The objectives are stated as follows:

$$\min_{\mathbf{X}} f^{EQ} = \widehat{BZI} \tag{11}$$

$$\min_{\mathbf{X}} f^{T} = \omega^{T}(T \circ S) \tag{12}$$

$$\min_{\mathbf{X}} f^{P} = c^{T} \cdot P^{G} \tag{13}$$

$$\min_{\mathbf{X}} f^{GPP} = \sum_{b'} \sum_{b} y_{bb'} \cdot a_{bb'} \tag{14}$$

$$\mathbf{p} = \mathbf{s} \cdot \mathbf{KD} \cdot (\mathbf{D} - \mathbf{LS}) \tag{15}$$

$$\sum_{g} s_{bg} = 1 \tag{16}$$

$$\sum_{b} s_{bg} = n_m \tag{17}$$

$$\sum_{m} n_m = NB \tag{18}$$

$$y_{bb'} = 1 - \sum_{g} s_{bg} \cdot s_{b'g} \tag{19}$$

$$\mathbf{p}^{min} \leq \mathbf{p} \leq \mathbf{p}^{max} \tag{20}$$

$$\mathbf{T} = M \cdot \mathbf{s} - (1 - \mathbf{s}) \cdot \hat{\mathbf{T}} \tag{21}$$

$$n_m - 1 = \textstyle\sum_{b'} FL_{bb'} - \sum_{b'} FL_{b'b}, \quad \forall b \in G \tag{22}$$

$$1 = \textstyle\sum_{b'} FL_{bb'} - \sum_{b'} FL_{b'b}, \quad \forall b \notin G \tag{23}$$

where $\mathbf{X}$ is a set of decision variables including binary sectionalization variables $\mathbf{s}$, binary line availability variables $\mathbf{y}$, power generation variables $\mathbf{p}$, restoration time $\mathbf{T}$, and load shedding variables $\mathbf{LS}$. In equation (14), $a_{bb'}$ is the elements of matrix $\mathbf{A} = [\, a_{bb'} \,]_{|NB| \times |NB|}$ which equals to one

if buses $b$ and $b'$ are connected and zero otherwise. $\mathbf{p} = [\,p_{gt}\,]_{|NG|\times|NT|}$ and $p_{gt}$ represents the power generated by BS unit $g$ at time $t$. Equation (15) is the load balance equation to ensure that the amount of power produced equals the total demand minus load shedding for each section. Matrix $\mathbf{KD} = [\,KD_{bd}\,]_{|NB|\times|ND|}$ is to indicate if demand node $d$ is located on network bus $b \in B$, where $d$ is a subset of $B$. For example, $KD_{31} = 1$ means that demand node 1 is connected to bus 3. Matrix $\mathbf{D} = [\,D_{dt}\,]_{|ND|\times|NT|}$ shows the amount of demand $d$ at time $t$. Equation (16) makes sure that each bus belongs to one and only one subsection. Equation (17) specifies the number of buses in each cluster and equation (18) ensures that the summation of different cluster's nodes do not exceed the total number of buses. Equation (19) is for the tie line configuration. If two buses are in the same subsection, then $y_{bb'}$ equals 0; otherwise, it equals 1. Equation 21 captures the restoration time, $\mathbf{T}$. The parameter $\hat{\mathbf{T}} = [\,\hat{T}_{bg}\,]_{NB\times NG}$ is a matrix representing the total energizing delay by bus $b$ and generator $g$. The amount of energizing delays are calculated for each bus by finding the shortest path between bus $b$ and generator $g$ using *Dijkstra's algorithm* [53] based on the electrical parameter of transmission lines, such as the series impedance of each transmission line [16]. The equations (22) and (23) ensure that each generator in each subsection provides a flow equal to the number of demand nodes in that subsection and each demand node receives a flow equal to one [54].

Note that constraint (19) is a quadratic equation, which can add a computational burden in solving the model. To overcome this issue, we linearize the constraint [55]:

$$-y_{bb'} - s_{mb} + s_{mb'} \leq 0 \tag{24}$$

$$-y_{bb'} + s_{mb} - s_{mb'} \leq 0 \tag{25}$$

The objective functions at the lower-level model are formulated like to the upper-level model excluding the GPP objective with the line power flow constraints as follows.

$$\min_{\mathbf{X}} f^{EQ} = LS_{max} - LS_{min} \tag{26}$$

$$\min_{\mathbf{X}} f^{T} = \omega^{T}(T \circ S) \tag{27}$$

$$\min_{\mathbf{X}} f^{P} = c^{T} \cdot P^{G} \tag{28}$$

$$\mathbf{p} = \mathbf{s} \cdot \mathbf{KD} \cdot (\mathbf{D} - \mathbf{LS}) \tag{29}$$

$$\mathbf{p}^{min} \leq \mathbf{p} \leq \mathbf{p}^{max} \tag{30}$$

$$|\mathbf{PL}_{l}| \leq PL^{max} \cdot (1 - y_{bb'}) \tag{31}$$

$$PL_{lt} - \frac{\theta_{bt} - \theta_{b't}}{x_l} \leq M.y_{bb'} \tag{32}$$

$$PL_{lt} - \frac{\theta_{bt} - \theta_{b't}}{x_l} \geq (-1).M.y_{bb'} \tag{33}$$

$$\theta_{ref,t} = 0 \tag{34}$$

$$LS_{max} \geq LS_{dt} \quad \forall d, t \tag{35}$$

$$LS_{min} \leq LS_{dt} \quad \forall d, t \tag{36}$$

Constraint (31) is to prevent overloading on each line. Constraints (32) to (34) are for transmission lines power flow.

Furthermore, a new constraint is added to re-evaluate the restoration time:

$$T_d \leq M \cdot LS_{dt} + CT_t \tag{37}$$

Equation (37) captures the exact moment of when having zero load shedding at each demand node. Instead of $f^T$, a weighted value of $T_d$ is maximized by the lower-level objective function. Hence, the restoration time objective term can be stated as

$$f'^{T} = -\mathbf{w}^{T} \cdot \mathbf{T} \tag{38}$$

where, $\mathbf{w} = [\, w_d \,]_{ND}$ is the cost of each hourly delay in the restoration of demand $d$. With this additional set of constraints (31)-(37), the optimal dispatched power flow is determined to give the final amount of unmet demand, **LS**, and the restoration time, **T**.

### *2.3. Equity based RCP Model*

The restoration plan by the GPP model has a connectivity matrix of the power grid as an input parameter. The connectivity matrix $\mathbf{A} = [a_{bb'}\,]_{NB \times NB}$

shows the connection status between each pair of buses via a binary parameter $a_{bb'}$. The diagonal elements $a_{bb}$ are always zero because it is assumed that a bus is not connected to itself. Although the line status can be observed via available sensors or phasor measurement units [56], some damaged lines may not be observable; hence, it is difficult to assess the status due to limited accessibility immediately after a disaster. Therefore, we consider the aftermath connectivity status of a power grid as an uncertain parameter and propose a RO method to develop a restoration plan accordingly. Wind intensity affects the line damage, which can be described through several factors such as the wind speed [30], the rainfall amount, the surge height, and the length of the forced outage [57]. A fragility curve (see Figure 2) is used to estimate the probability of the line failure for a given wind speed [58]. Because it is a

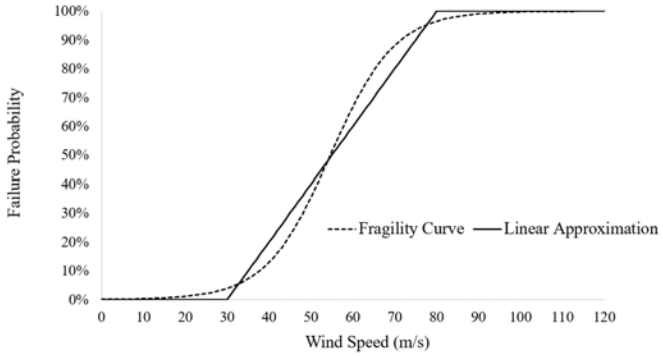


Figure 2: Fragility curve of high voltage transmission lines [30]

non-linear function, it is often approximated by a linear function associated with a high-voltage transmission line [48]. In this paper, the line status for a given simulated scenario of a wind speed is determined by the following rule:

$$\begin{cases} a_{bb'} = 1 & P(\omega_l) \geq \mu_l,\ \ l \sim (b, b'),\ \ \forall l \\ a_{bb'} = 0 & P(\omega_l) < \mu_l,\ \ l \sim (b, b'),\ \ \forall l \end{cases} \tag{39}$$

where, for line $l$, $P(\omega_l)$ is the probability of line failure for wind speed $\omega_l$ and $\mu_l$ is a tolerance threshold against the wind intensity. The set of wind speed scenarios are generated by a Monte Carlo simulation [59], where a Weibull distribution is used for the wind speed based on the goodness-of-fit test. The resulting line availability scenarios are tabulated as $\mathbf{A}^s = [\, {a_{bb'}}^s \,]_{NB \times NB}$.

The goal of the RO model is to find an optimal solution to minimize the worst possible scenario that could happen in reality. Since the uncertain

parameter appears in the objective function of the upper-level model only, the objective function of the GPP is revised as

$$f_{rev}^{GPP} = \min_{\mathbf{X}} \max_{s} f_s^{GPP} \tag{40}$$

For simplicity in the implementation of the optimization model, we reformulate this objective function by introducing a new variable $z$, an upper bound of $\max_s f_s^{GPP}$, and add the following constraint to the model:

$$z \geq \sum_{(b,b')\sim l} a_{bb'}^s \cdot y_{bb'}, \forall s \tag{41}$$

Since parameter $a_{bb'}^s$ is binary, we can represent the worst-case by replacing $a_{bb'}^s$ with $\Pi_s a_{bb'}^s$ as:

$$z = \sum_{(b,b')\sim l} (\Pi_s a_{bb'}^s).y_{bb'} \tag{42}$$

This reformulation works because if a particular line between buses $b$ and $b'$ becomes unavailable even for one scenario $i$, $a_{bb'}^i$ becomes zero; consequently, $\Pi_s a_{bb'}^s = 0$. We can use this idea to capture the worst-case scenario simply by multiplying all $a_{bb'}^s$, i.e., $\Pi_s a_{bb'}^s$.

The resulting model is a linear robust counterpart (RCP) problem with four objectives.

$$\min_{\mathbf{X}} f^{LS} \tag{43}$$

$$\min_{\mathbf{X}} f^{T} \tag{44}$$

$$\min_{\mathbf{X}} f^{P} \tag{45}$$

$$\min_{\mathbf{X}} z \tag{46}$$

$$s.t. \qquad Constraints \;\; (15)-(18), (20)-(21) \tag{47}$$

Like the GPP model, the RCP is a bi-level model that can be solved through an iterative optimization process. At each iteration, upper- and lower-level models are solved using the preemptive goal programming method considering the different unit scales and priority among the objective terms [13].

*2.4. Accounting for Planner's Risk Tolerance via Degree of Conservativeness*

A drawback of solving the power restoration problem using the worst-case RCP model is that the obtained solution can be too conservative with respect to the actual realization of a disaster (i.e., hurricane). This can become particularly problematic if the generated scenarios exhibit a wide range of variability having only a few data points far away from the rest of the data. As the RCP is designed to find a solution satisfying all scenarios, the resulting solution may be unnecessarily conservative because those less common scenarios do not likely occur in reality. To address this issue and provide the decision maker (DM) with the flexibility in obtaining a solution considering the DM's risk tolerance, we propose a concept "degree of conservativeness" ($\delta$) of a solution in a RCP model. Without using $\delta$, a RCP model will assume a line is failed unless all scenarios (100%) of an uncertain parameter show the line is working. Therefore, $\delta$ is a control parameter for a DM to use so that a line will be considered failed in the optimization model if less than $\delta \times 100$ percent of the generated scenarios show the line is operable. For example, suppose the DM sets $\delta$ to 0.9. This means a particular line will be assumed working in the optimization model only if more than 90% of the generated scenarios show the line being operable. This parameter is important because it allows the model to be customizable depending on the DM's risk preference. If the DM does not want to take any risk with respect to the realization of the line failure (i.e., risk averse), the $\delta$ value should be 1 (or 100%), i.e., the worst-case RO. However, plans associated with the worst-case scenario may result in inefficient use of resources because such extreme cases may be less likely realized in a real situation. Hence, the DM may want to choose a value less than 100% so that the resulting plan should work according to the selected level of $\delta$.

As we explained how to pre-calculate $\Pi_s a^s_{bb'}$ in the previous section, a similar implementation can be used to calculate the line connectivity matrix ($\hat{a}^\delta_{bb'}$) according to the degree of conservativeness. For a specific line between buses $b$ and $b'$, if less than $\delta$ percent of all generated scenarios show that line is available, $\hat{a}^\delta_{bb'}$ would be equal to zero; otherwise, it would be equal to one (i.e., 100%). Hence, $z$ (42) can be redefined as

$$z = \sum_{(b,b')\sim l} a^\delta_{bb'} . y_{bb'} \tag{48}$$

Then, the RCP model in Section 2.3 with this revised $z$ is solved to optimize a plan considering the degree of conservativeness.

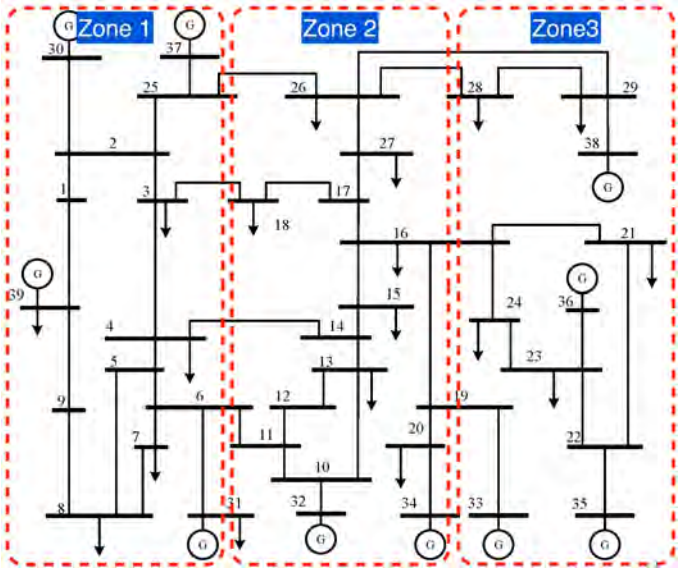


Figure 3: The projected IEEE 39-bus test case on the wind speed zones

## 3. Results and Discussions

Two case studies are prepared based on the IEEE 14-bus, and 39-bus test systems considering an appropriate number of BS generators [13]. The National Institute of Standards and Technology (NIST) provides 999 scenarios of a simulated hurricane at the coastline of the Gulf of Mexico [59, 60]. Therefore, we use the data to generate hurricane wind speed scenarios for this study. The wind speed is provided for 10 meters above the ground level at every 50 miles. The location of each transmission line among the zones is determined by the zone which covers most of the line's length, as illustrated in Figure 3.

In this section, we analyze the results from different aspects, including load shedding amount, load shedding percentage, load shedding standard deviation across scenarios, equity index, and degree of conservativeness. The results are examined under four different setups: the GPP model without equity consideration, the EA-GPP model with equity consideration, the RCP model without equity consideration, and the EA-RCP model with equity consideration.

Black start generators are used for rapid power restoration, but their capacity may not be sufficient enough to meet all demand, leading to inevitable

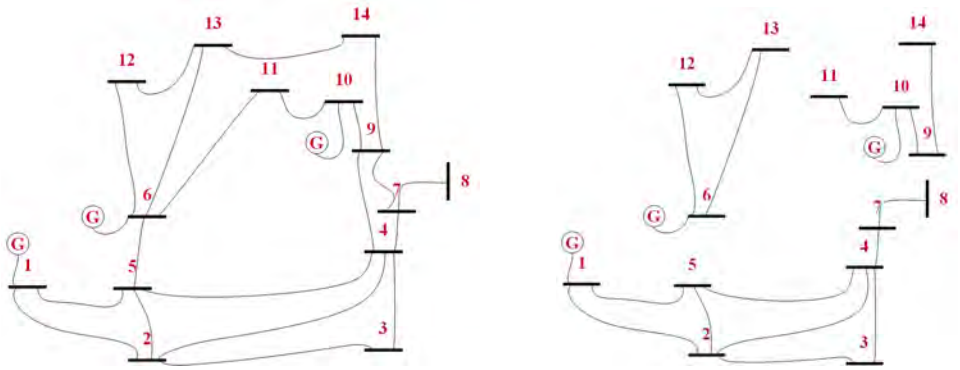


(a) The IEEE 14-bus test case abstracted as a graph

(b) The partitioned IEEE 14-bus test case

Figure 4: Graph shape of the 14-bus power network

load shedding, particularly during peak demand hours. The restoration process is modeled over a time horizon of 24 hours, with decisions made at 1-hour intervals.

Tables 1 and 2 summarize the overall load-shedding outcomes across different models. One key observation is that the total load shedding amount remains the same in the GPP and RCP models compared to the EA-GPP and EA-RCP models. This happens because the system fully utilizes the available generation capacity to meet demand, ensuring that all possible power generation is used. However, in other scenarios where excess generation is available, the load shedding amount may vary between models.

While the absolute load shedding amount remains unchanged, the percentage of load shedding differs between the equity-aware and non-equity models. The equity-aware models, EA-GPP and EA-RCP, result in a lower average load-shedding percentage compared to their non-equity counterparts. This occurs because the equity-aware objectives aim to minimize disparities in power restoration across different demand buses, leading to a more balanced distribution of available power. The reduction in load-shedding percentage indicates that these models prioritize fairness, even if the total amount of load shedding remains the same.

Another key result is the impact of robustness on load shedding variability. In the GPP-based models, the standard deviation of load shedding amount is nonzero across different scenarios. This is due to the fact that these models do not account for the stochasticity of transmission line availability, meaning that restoration outcomes vary across different failure sce-

Table 1: RCP and GPP models comparison

| Opt. Models | Test Case | Non-Equity Models | | | |
|---|---|---|---|---|---|
| | | LS Amount | LS S.D. | LS Percentage | LS Percentage S.D. |
| GPP | 14-bus | 5.41 | 2.80 | 28% | 10% |
| | 39-bus | 43.15 | 9.04 | 18% | 1% |
| RCP | 14-bus | 4.74 | 0 | 15% | 0% |
| | 39-bus | 13.97 | 0 | 11% | 0% |

Table 2: EA-GPP and EA-RCP models comparison

| Opt. Models | Test Case | Equity Models | | | |
|---|---|---|---|---|---|
| | | LS Amount | LS S.D. | LS Percentage | LS Percentage S.D. |
| GPP | 14-bus | 4.74 | 2.80 | 25% | 11% |
| | 39-bus | 43.15 | 9.04 | 17% | 2% |
| RCP | 14-bus | 4.74 | 0 | 5% | 0% |
| | 39-bus | 13.97 | 0 | 10% | 0% |

narios. In contrast, the RCP-based models show a standard deviation of zero in load shedding. This indicates that the robust counterpart model successfully accounts for uncertainties in transmission line failures, leading to a consistent restoration strategy across all scenarios. The robustness ensures that, regardless of specific failure scenarios, the system adapts to worst-case disruptions and maintains stability in power restoration.

Tables 1 and 2 highlights these results in detail, showing how equity-aware and robust models influence load shedding patterns across different test cases. The results demonstrate that robust optimization stabilizes outcomes across different failure scenarios, while equity-aware objectives reduce disparities in power distribution, leading to a more socially fair restoration process.

Table 3 summarizes the equity performance of the models. The equity objective in the upper-level mathematical model was to minimize Theil's T index, while the lower-level objective was to minimize the equity gap. The table presents these metrics for different model configurations. Although comparing equity metrics between the GPP and RCP models is not meaningful due to their structural differences, the comparison between non-equity and equity-aware models reveals significant improvements in both metrics.

Theil's T index ranges from 0 to $\infty$, where values closer to 0 indicate better equity. In both the GPP and RCP models, the equity-aware versions achieve a lower Theil's T index, indicating improved fairness in power distribution. Similarly, the average equity gap, defined as the average load-

Table 3: Comparison of Theil's T Index and Equity Gap for Non-Equity and Equity Models

| Metric | Model | Equity Consideration | |
|---|---|---|---|
| | | Equity | Non-Equity |
| Average Theil's T Index | GPP | 0.5242 | 1.4087 |
| | RCP | 1.1311 | 1.9993 |
| Average Equity Gap | GPP | 42% | 67% |
| | RCP | 56% | 66% |

shedding percentage gap within sections across different scenarios, is lower in the equity-aware models. This reduction highlights the model's ability to enhance social equity in power restoration. However, given the multi-objective nature of the problem, achieving perfect equity is often not feasible.

### *3.1. Analysis on the degree of conservativeness*

So far, in Tables 1 and 2, we have presented the performance of the GPP model and the best-performing RCP model. Now, we analyze the average load-shedding amount and percentage across all degrees of conservatism. The degree of conservatism, denoted as $\delta$, is defined as the threshold that determines whether a transmission line is considered available based on its failure probability across all scenarios. Specifically, if the proportion of scenarios in which a transmission line remains operational falls below this threshold, the line is deemed unavailable in the optimization process.

For extreme values of $\delta$, consider $\delta = 1$. This implies that if, out of 999 wind speed scenarios, a specific transmission line is available in 998 scenarios but fails in just one, the ratio $\frac{998}{999} < 1$, meaning that the line is considered unavailable. Thus, $\delta = 1$ represents the worst-case scenario, where even a single failure scenario results in the exclusion of a transmission line.

Conversely, if $\delta = 0$, all lines are considered available because no ratio can be lower than zero, i.e., $\frac{n}{999} \not< 0 \quad \forall n \in \mathbb{Z}^+$. This extreme case is equivalent to the deterministic GPP model, where no transmission line failures are assumed. The degree of conservatism can take any value between 0 and 1, allowing for a balance between worst-case robustness and optimistic planning.

When $\delta = 0$, the model behaves as a deterministic system, leading to greater fluctuations in output across different wind speed scenarios. At $\delta = 1$, the model becomes overly conservative, limiting the number of available transmission lines, even when many are operational in reality. This excessive conservatism results in suboptimal performance and unnecessary restrictions.

By gradually increasing $\delta$, we reach a sweet spot where fluctuations are minimized while maintaining strong performance metrics.

Figures 5a and 5b validate this observation. Figure 5a illustrates the average load shedding percentage across 10 degrees of conservatism, increasing in increments of 0.1, for the 14-bus test case. The optimal range appears to be between $\delta = 0.7$ and $\delta = 0.9$, where fluctuations decrease and load-shedding performance improves. Another key takeaway from this figure is that the equity-aware model consistently results in a lower load-shedding percentage compared to the non-equity model across nearly all conservatism levels, demonstrating the robustness of the equity-aware formulation.

Figure 5b presents the average load shedding amount across different degrees of conservatism. The trend confirms that the minimum load shedding occurs between $\delta = 0.7$ and $\delta = 0.9$, reinforcing the conclusion that this range provides the most balanced trade-off between conservatism and system performance. We will discuss about the fluctuations later.

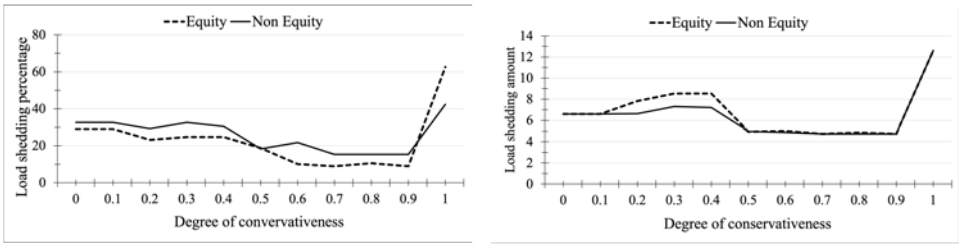


(a) (b)

Figure 5: The effect of changing degree of conservativeness on average load shedding **(a)** percentage and **(b)** amount for 14-bus test case.

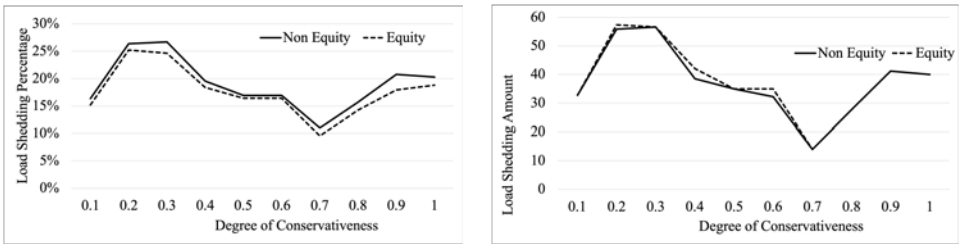


(a) (b)

Figure 6: The effect of changing degree of conservativeness on average load shedding **(a)** percentage and **(b)** amount for 39-bus test case.

Figures 6a and 6b present the same analysis for the 39-bus test case, il-

lustrating the trends in load-shedding percentage and load-shedding amount across different degrees of conservatism. Similar to the 14-bus case, both metrics reach their minimum values around $\delta = 0.7$, reinforcing the observation that this range provides the most effective trade-off between robustness and performance.

To further demonstrate the robustness of our model, we analyze the standard deviations of load shedding across all scenarios at different degrees of conservatism. Figures 7a and 7b summarize these results. In Figure 7a, we observe that for $\delta \geq 0.7$, the standard deviation of load-shedding percentage across all scenarios converges to approximately zero. This indicates that as we approach $\delta = 1$, the model becomes increasingly robust, with the outputs becoming less sensitive to variations in wind speed scenarios.

A similar trend is observed in Figure 7b, which depicts the standard deviation of load-shedding amount across different conservatism levels. The decreasing variability confirms that the model's decisions become more stable and resilient as $\delta$ increases, ensuring that the restoration strategy is less affected by individual failure scenarios. These results highlight the model's ability to adapt to uncertainty while maintaining consistent performance at higher levels of conservatism.

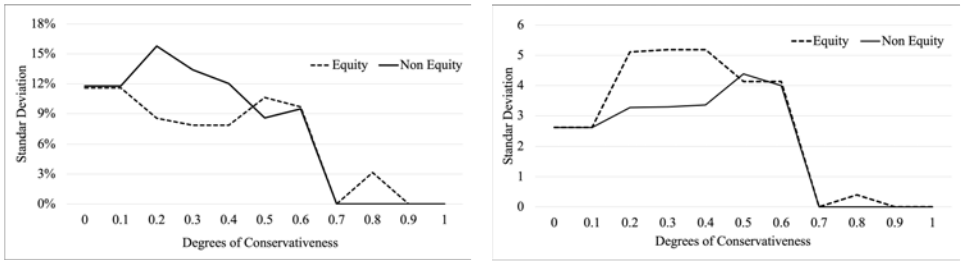


(a) (b)

Figure 7: Standard Deviation vs. degree of conservativeness for **(a)** load shedding percentage and **(b)** load shedding amount.

### *3.2. Equity Awareness and Degrees of Conservativeness*

This section compares the performance of different optimization models introduced in this paper, including the equity aware robust model (EA-RCP), non-equity aware robust model (RCP), equity aware deterministic model (EA-GPP), and non-equity aware deterministic model (GPP). Figure 5 shows comparisons between EA-RCP and RCP for (a) the average load shedding percentage and (b) the average load shedding amount over different

degrees of conservativeness. Each data point represents an average value of twenty different scenarios.

The EA-RCP model's purpose is to restore power up to a certain level to ensure all nodes have at least some amount of power. Therefore, the EA-RCP model may have a higher average load shedding amount to achieve a lower average load shedding percentage. Two observations can be made from this experiment.

First, for $\delta \in [0, 0.9]$, the average load shedding percentage for the EA-RCP model was lower than the RCP model by average of 5.6 %,as seen in Figure 5a. This means EA-RCP ensures all nodes have some level of restored power, while the RCP model just focuses on minimizing the total load shedding amount. Consequently, the total amount of load shedding from the RCP may be lower than that of the EA-RCP. This comparison is shown in Figure 5b for different $\delta$ values. As expected, the RCP solution has a slightly lower load shedding amount, but the difference is negligible for $\delta \in (0.1, 0.5)$.

We further discuss this with an example in Figure 9. This example is for three load nodes (2, 3, and 4) in the last 6 hours of our restoration time horizon with $\delta = 0.8$. Figure 9a shows the load shedding performance for the EA-RCP model, and Figure 9b shows it for the RCP model. The total load shedding amount for both of the models was equal throughout the time horizon. However, the average load shedding percentage was much lower for the EA-RCP model. The reason for this is that nodes 3 and 4 have lower demand than node 2. The RCP model tries to restore the power of nodes that have a higher load demand so that the total load-shedding amount will be minimized. Thus we observed that nodes 3 and 4 have 100% load shedding most of the time. But, the EA-RCP model put all the load shedding on node 2. It is because the priority here was restoring loads to a certain operational percentage. So, putting all the loads on node 1 would be a better decision towards equity since nodes 3 and 4 were restored completely, and node 1 has a certain amount of power to operate.

The second observation is how using the degrees of conservativeness concept affects load shedding among different models. The solution of the robust model does not always lead to the best results for load shedding since the RO is very conservative in dealing with an uncertain model parameter. Figures 5 show that choosing a degree of conservativeness between 0.5 to 0.9 leads to better load shedding performance.

Figure 8a shows two box plots of the average load shedding percentage over different degrees of conservativeness for the EA-RCP and RCP models. Note that $\delta = 0$ is equivalent to the GPP model being the least conservative

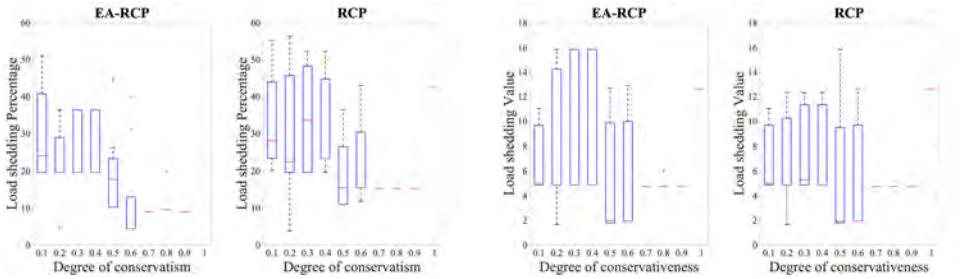


(a) Load shedding percentage box-plot over the different degrees of conservativeness

(b) Load shedding amount box-plot over the different degrees of conservativeness

Figure 8: The effect of changing degree of conservativeness on the dispersion of load shedding

regarding the unknown power line availability.

| Load \ Hour | | 19 | 20 | 21 | 22 | 23 | 24 |
|---|---|---|---|---|---|---|---|
| 2 | Amount | 66.62 | 64.19 | 64.19 | 66.62 | 52 | 15.45 |
| | Percentage | 66% | 64% | 64% | 66% | 55% | 20% |
| 3 | Amount | 0 | 0 | 0 | 0 | 0 | 0 |
| | Percentage | 0% | 0% | 0% | 0% | 0% | 0% |
| 4 | Amount | 0 | 0 | 0 | 0 | 0 | 0 |
| | Percentage | 0% | 0% | 0% | 0% | 0% | 0% |
| Total LS amount | | 66.62 | 64.19 | 64.19 | 66.62 | 52.00 | 15.45 |
| Average LS Percentage | | 22% | 21% | 21% | 22% | 18% | 7% |

(a) EA-RCP solution: load-shedding

| Load \ Hour | | 19 | 20 | 21 | 22 | 23 | 24 |
|---|---|---|---|---|---|---|---|
| 2 | Amount | 7.4 | 5.6 | 5.6 | 7.4 | 0 | 0 |
| | Percentage | 7% | 6% | 6% | 7% | 0% | 0% |
| 3 | Amount | 51.1 | 50.55 | 50.55 | 51.1 | 44.4 | 9.16 |
| | Percentage | 100% | 100% | 100% | 100% | 93% | 23% |
| 4 | Amount | 8.12 | 8.04 | 8.04 | 8.12 | 7.6 | 6.29 |
| | Percentage | 100% | 100% | 100% | 100% | 100% | 100% |
| Total LS amount | | 66.62 | 64.19 | 64.19 | 66.62 | 52.00 | 15.45 |
| Average LS Percentage | | 69% | 69% | 69% | 69% | 64% | 41% |

(b) RCP solution: load-shedding

Figure 9: An example final load shedding for load nodes 2, 3, and 4 at time horizons 19-24 for (a) EA-RCP and (b) RCP

Two observations can be made from this figure. First, the variation of the load shedding percentage for EA-RCP is lower than RCP as expected. Second, as we increase the degree of conservativeness, the variation inside each model decreases. This means that the model becomes more robust as the degree of conservativeness is increased. On the other hand, Figure 8b demonstrates the load shedding amount box plot over the different degrees of conservativeness between EA-RCP and RCP. The EA model exhibits a higher variance in the load shedding amount. This is because minimizing the amount of load shedding does not take high priority in the EA model.

Figure 10 is a radar plot to compare performance of the four different models. The results for the RCP model are based on $\delta = 0.9$. Figure 10b shows that the EA-RCP model achieved the lowest average load shedding percentage compared to the other models (EA-GPP, GPP, EA-RCP, and RCP). In the case of the load shedding amount, figure 10a shows that the


(a) Load shedding amount (b) Load shedding percentage

Figure 10: Radar diagram for comparison between four different models

RCP models outperform GPP models. Also, the EA-RCP and RCP have the same amount of load shedding for $\delta = 0.9$. Overall, the EA-RCP outperformed other models by having the lowest load shedding amount and load shedding percentage.

## 4. Conclusion

Fast restoration of power grids is essential to build resilient power systems for our society as many vital infrastructures depend on reliable electricity for normal operations. This paper presented optimization models considering equity in power restoration dealing with the aftermath of a disaster. We began with a revised optimization model formulation under no parameter uncertainty assumption, followed by equity-aware models and the RCP model formulation. Our revised model addresses the infeasibility problem found in the existing model in the literature. Then, a worst-case RCP approach was proposed to address uncertainty on the availability of the transmission lines caused by an extreme event. The concept of degree of conservativeness also proposed to take decision makers risk tolerance into account. In theory, a worst-case RCP generates a solution satisfying various possible realizations of the event. As a result, the solutions can be unnecessarily conservative and call for over-commitment of scarce resources during the restoration process. Therefore, the concept of degree of conservativeness was introduced so that the decision makers can participate in the plan generation depending on their risk-taking preference. In the proposed model, the degree of conservativeness can be controlled by parameter $\delta$. Numerical experiments are made to test the performance of the GPP, RCP, EA-GPP, and EA-RCP models using three *IEEE* test bus instances: 14, 39, and 118. We made a few notable observations from the results. First, we started to compare

GPP model and RCP model regarding their load-shedding and restoration time performance. Then we did a conservativeness analysis on EA-RCP and RCP models. the results showed that along different degrees of conservativeness the load-shedding performances are different. for 14-bus test case $\delta \in [0.1, 0.9]$ gave us the best performance. We also showed the RCP-based models converged fast, and its performance was comparable to the GPP based on the cases used in this study. Furthermore, we considered equity criteria into account and observed that equity-aware model performs better considering load-shedding percentage as the performance metric. A numerical example was proposed to discuss the benefit of using equity-aware model to restore power to a certain operational level for each node. Regarding the load-shedding amount, EA-RCP model worked very close to RCP.

This paper assumed known demand and a pre-determined amount of power to support the network. However, these parameters can be uncertain in practice. Hence, future work can extend this paper to consider uncertainty in those input parameters in an RCP model or data-driven optimization model.

## References


[1] M. Hand, Millions in florida and georgia without electricity after irma, repairs expected to take weeks, Online, accessed: 2017-09-12 (2017).
URL `https://archive.thinkprogress.org/irma-power-outages-de70ba460ae2/`

[2] M. Najarian, G. J. Lim, Optimizing infrastructure resilience under budgetary constraint, Reliability Engineering & System Safety 198 (2020) 106801.

[3] R. J. Campbell, S. Lowry, Weather-related power outages and electric system resiliency, Tech. Rep. R42696, Congressional Research Service, Library of Congress (2012).
URL `https://sgp.fas.org/crs/misc/R42696.pdf`

[4] U.S. Energy Information Administration, Average frequency and duration of electric distribution outages vary by states (2018).
URL `https://www.eia.gov/todayinenergy/detail.php?id=35652`

[5] K. Wootton, E source market research reveals that power outages cost businesses over $27 billion annually, winter storm jonas makes it worse, Online, accessed: 2016-01-27 (2016).

URL https://www.esource.com/ES-PR-Outages-2016-01/Press-Release/Outages

[6] A. L. Beck, E. J. Cha, W. G. Peacock, Incorporation of equity into infrastructure decision-making: Development of an equity metric for infrastructure retrofitting, in: Proceedings of the 14th International Conference on Applications of Statistics and Probability in Civil Engineering (ICASP14), Dublin, Ireland, 2023, p. N/A.

[7] B. K. Sovacool, M. H. Dworkin, Global energy justice, Cambridge University Press, 2014.

[8] B. K. Sovacool, M. Burke, L. Baker, C. K. Kotikalapudi, H. Wlokas, New frontiers and conceptual frameworks for energy justice, Energy Policy 105 (2017) 677–691.

[9] S. Bouzarovski, N. Simcock, Spatializing energy justice, Energy Policy 107 (2017) 640–648.

[10] R. J. Heffron, D. McCauley, The concept of energy justice across the disciplines, Energy Policy 105 (2017) 658–667.

[11] S. Abbasi, M. Barati, G. Lim, A multi-objective mpec model for disaster management of power system restoration, in: IIE Annual Conference. Proceedings, Institute of Industrial and Systems Engineers (IISE), 2017, pp. 872–877.

[12] S. Abbasi, M. Barati, G. J. Lim, A parallel sectionalized restoration scheme for resilient smart grid systems, IEEE Transactions on Smart Grid 10 (2) (2017) 1660–1670.

[13] S. Abbasi, M. Barati, G. Lim, A GPP-based sectionalization toward a fast power transmission system restoration, in: International Conference on Applied Human Factors and Ergonomics, Springer, 2017, pp. 11–21.

[14] A. Golshani, W. Sun, Q. Zhou, Q. P. Zheng, Y. Hou, Incorporating wind energy in power system restoration planning, IEEE Transactions on Smart Grid 10 (1) (2017) 16–28.

[15] G. Patsakis, D. Rajan, I. Aravena, J. Rios, S. Oren, Optimal black start allocation for power system restoration, IEEE Transactions on Power Systems 33 (6) (2018) 6766–6776.

[16] W. Liu, Z. Lin, F. Wen, C. Chung, Y. Xue, G. Ledwich, Sectionalizing strategies for minimizing outage durations of critical loads in parallel power system restoration with bi-level programming, International Journal of Electrical Power & Energy Systems 71 (2015) 327–334.

[17] Y. Zhao, Z. Lin, Y. Ding, Y. Liu, L. Sun, Y. Yan, A model predictive control based generator start-up optimization strategy for restoration with microgrids as black-start resources, IEEE Transactions on Power Systems 33 (6) (2018) 7189–7203.

[18] M. Adibi, P. Clelland, L. Fink, H. Happ, R. Kafka, J. Raine, D. Scheurer, F. Trefny, Power system restoration-a task force report, IEEE Transactions on Power systems 2 (2) (1987) 271–277.

[19] C. Wang, V. Vittal, K. Sun, Obdd-based sectionalizing strategies for parallel power system restoration, IEEE Transactions on Power Systems 26 (3) (2010) 1426–1433.

[20] N. Fountas, N. Hatziargyriou, C. Orfanogiannis, A. Tasoulis, Interactive long-term simulation for power system restoration planning, IEEE transactions on power systems 12 (1) (1997) 61–68.

[21] L. Sun, C. Peng, J. Hu, Y. Hou, Application of type 3 wind turbines for system restoration, IEEE Transactions on Power Systems 33 (3) (2017) 3040–3051.

[22] N. Ahmadian, G. J. Lim, J. Cho, S. Bora, A quantitative approach for assessment and improvement of network resilience, Reliability Engineering & System Safety 200 (2020) 106977.

[23] Y. Liu, R. Fan, V. Terzija, Power system restoration: a literature review from 2006 to 2016, Journal of Modern Power Systems and Clean Energy 4 (3) (2016) 332–341.

[24] S. Thiébaux, M.-O. Cordier, et al., Supply restoration in power distribution systems—a benchmark for planning under uncertainty, in: Pre-Proceedings of the 6th European Conference on Planning (ECP-01), 2001, pp. 85–96.

[25] C. Zhang, Y.-F. Li, H. Zhang, Y. Wang, Y. Huang, J. Xu, Distributionally robust resilience optimization of post-disaster power system considering multiple uncertainties, Reliability Engineering & System Safety 251 (2024) 110367.

[26] R. N. Allan, et al., Reliability evaluation of power systems, Springer Science & Business Media, 2013.

[27] A. Khayatian, M. Barati, G. J. Lim, Integrated microgrid expansion planning in electricity market with uncertainty, IEEE Transactions on Power Systems 33 (4) (2017) 3634–3643.

[28] W. Su, J. Wang, J. Roh, Stochastic energy scheduling in microgrids with intermittent renewable energy resources, IEEE Transactions on Smart Grid 5 (4) (2013) 1876–1883.

[29] Q. Xie, X. Liu, S. Wu, Resilience-based optimisation framework for post-earthquake restoration of power systems, Reliability Engineering & System Safety 257 (2025) 110808.

[30] M. Panteli, P. Mancarella, The grid: Stronger, bigger, smarter?: Presenting a conceptual framework of power system resilience, IEEE Power and Energy Magazine 13 (3) (2015) 58–66.

[31] Y. Liu, C. Singh, A methodology for evaluation of hurricane impact on composite power system reliability, IEEE Transactions on Power Systems 26 (1) (2010) 145–152.

[32] M. Ouyang, L. Duenas-Osorio, Multi-dimensional hurricane resilience assessment of electric power systems, Structural Safety 48 (2014) 15–24.

[33] S. R. Fahim, S. Muyeen, M. A. Mannan, S. K. Sarker, S. K. Das, N. Al-Emadi, Uncertainty awareness in transmission line fault analysis: A deep learning based approach, Applied Soft Computing 128 (2022) 109437.

[34] J. H. Roh, M. Shahidehpour, L. Wu, Market-based generation and transmission planning with uncertainties, IEEE Transactions on Power Systems 24 (3) (2009) 1587–1598.

[35] P. Jirutitijaroen, C. Singh, Reliability constrained multi-area adequacy planning using stochastic programming with sample-average approximations, IEEE Transactions on Power Systems 23 (2) (2008) 504–513.

[36] A. J. Conejo, X. Wu, Robust optimization in power systems: a tutorial overview, Optimization and Engineering 23 (4) (2022) 2051–2073.

[37] R. Wang, P. Wang, G. Xiao, A robust optimization approach for energy generation scheduling in microgrids, Energy Conversion and Management 106 (2015) 597–607.

[38] Y. Zhang, N. Gatsis, G. B. Giannakis, Robust energy management for microgrids with high-penetration renewables, IEEE transactions on sustainable energy 4 (4) (2013) 944–953.

[39] A. Prékopa, Stochastic programming, Vol. 324, Springer Science & Business Media, 2013.

[40] P. Kall, S. W. Wallace, P. Kall, Stochastic programming, Springer, 1994.

[41] S. Lei, J. Wang, C. Chen, Y. Hou, Mobile emergency generator prepositioning and real-time allocation for resilient response to natural disasters, IEEE Transactions on Smart Grid 9 (3) (2016) 2030–2041.

[42] H.-G. Beyer, B. Sendhoff, Robust optimization–a comprehensive survey, Computer methods in applied mechanics and engineering 196 (33-34) (2007) 3190–3218.

[43] M. Ansari, J. S. Borrero, L. Lozano, Robust minimum-cost flow problems under multiple ripple effect disruptions, INFORMS Journal on Computing 35 (1) (2023) 83–103.

[44] A. Golshani, W. Sun, Q. Zhou, Q. P. Zheng, J. Wang, F. Qiu, Coordination of wind farm and pumped-storage hydro for a self-healing power grid, IEEE Transactions on Sustainable Energy 9 (4) (2018) 1910–1920.

[45] X. Bai, G. Lim, H.-P. Wieser, M. Bangert, D. Grosshans, R. Mohan, W. Cao, Robust optimization to reduce the impact of biological effect variation from physical uncertainties in intensity-modulated proton therapy, Physics in Medicine & Biology 64 (2) (2019) 025004.

[46] G. J. Lim, M. Rungta, A. Davishan, A robust chance constraint programming approach for evacuation planning under uncertain demand distribution, IISE Transactions 51 (6) (2019) 589–604.

[47] A. Khabazian, M. Zaghian, G. J. Lim, A feasibility study of a risk-based stochastic optimization approach for radiation treatment planning under setup uncertainty, Computers & Industrial Engineering 135 (2019) 67–78.

[48] M. Panteli, C. Pickering, S. Wilkinson, R. Dawson, P. Mancarella, Power system resilience to extreme weather: fragility modeling, probabilistic impact assessment, and adaptation measures, IEEE Transactions on Power Systems 32 (5) (2016) 3747–3757.

[49] F. F. Wu, A. Monticelli, Analytical tools for power system restoration-conceptual design, IEEE Transactions on Power Systems 3 (1) (1988) 10–26.

[50] M. Adibi, L. Fink, Power system restoration planning, IEEE Transactions on Power Systems 9 (1) (1994) 22–28.

[51] H. A. Taha, Operations Research: An Introduction, $10^{th}$ Ed., Pearson, 2017.

[52] H. Theil, Economics and Information Theory, North-Holland Publishing Company, 1967.

[53] S. E. Dreyfus, An appraisal of some shortest-path algorithms, Operations Research 17 (3) (1969) 395–412.

[54] L. Wolsey, Integer Programming, 2nd ed., John Wiley & Sons, Inc, 2020.

[55] F. Glover, Improved linear integer programming formulations of nonlinear integer problems, Management Science 22 (4) (1975) 455–460.

[56] F. Galvan, S. Mandal, M. Thomas, Phasor measurement units (pmu) instrumental in detecting and managing the electrical island created in the aftermath of hurricane gustav, in: 2009 IEEE/PES Power Systems Conference and Exposition, IEEE, 2009, pp. 1–4.

[57] N. Lin, J. A. Smith, G. Villarini, T. P. Marchok, M. L. Baeck, Modeling extreme rainfall, winds, and surge from hurricane isabel (2003), Weather and forecasting 25 (5) (2010) 1342–1361.

[58] Y. Yang, Y. Xin, J. Zhou, W. Tang, B. Li, Failure probability estimation of transmission lines during typhoon based on tropical cyclone wind model and component vulnerability model, in: 2017 IEEE PES Asia-Pacific Power and Energy Engineering Conference (APPEEC), IEEE, 2017, pp. 1–6.

[59] M. E. Batts, E. Simiu, L. R. Russell, Hurricane wind speeds in the united states, Journal of the Structural Division 106 (10) (1980) 2001–2016.

[60] National Institute of Standards and Technology (NIST), Extreme wind speed data sets: Hurricane wind speeds, accessed: 2025-02-26 (2005). URL https://www.itl.nist.gov/div898/winds/hurricane.htm